Intrinsic inhomogeneity in a $(La_{0.4}Eu_{0.6})_{0.7}Pb_{0.3}MnO_3$ single crystal: Magnetization, transport, and electron magnetic resonance studies

N. Volkov, G. Petrakovskii, K. Patrin, K. Sablina, E. Eremin, V. Vasiliev, A. Vasiliev, and M. Molokeev
L. V. Kirensky Institute of Physics SB RAS, Krasnoyarsk 660036, Russia

P. Böni and E. Clementyev
Physics-Department E21, Technical University of Munich, D-85747 Garching, Germany
(Received 26 August 2005; revised manuscript received 13 January 2006; published 1 March 2006)

Conventional magnetic and transport measurements of the melt-grown mixed-valence manganite $(La_{0.4}Eu_{0.6})_{0.7}Pb_{0.3}MnO_3$ have been supplemented by a magnetic resonance study. The experimental data support the model of two magnetic phases coexisting in the crystal volume. At a temperature T^*, which is well above Curie temperature T_C, ferromagnetic clusters appear in the sample. These ferromagnetic regions possess a higher conductivity in comparison with the paramagnetic background (majority phase). On cooling through T_C, the magnetization of the spatially confined ferromagnetic clusters of the minority phase freezes in random directions with respect to the magnetization of the ferromagnetic majority phase due to the difference of the exchange interactions at the phase boundaries from the intraphase interactions in sign and value. Such a mixed state is responsible for the observed magnetic glassylike behavior of the system that is characteristic of inhomogeneous magnets. The fluctuations of the magnetic coupling value and sign in the sample volume are related to strong competition between the ferromagnetic and antiferromagnetic exchange interactions, which, in turn, results from the quenched disorder caused by the random chemical replacement of the perovskite *A* site of the manganite. A phase-separation state comprised of two different ferromagnetic phases has been used to account for the colossal magnetoresistance phenomenon and the magnetic-field-driven nonlinear conduction found in the crystal.

DOI: 10.1103/PhysRevB.73.104401 PACS number(s): 75.50.Lk, 75.30.Cr, 76.50.+g

I. INTRODUCTION

Mixed-valence manganese oxides $R_{1-x}R'_xMnO_3$ (R =La,Nd,Pr,Sm, etc., and R'_x=Ca,Sr,Ba,Pb, etc.), well known as manganites, continue to be a subject of intense investigations aimed at the study of physical properties of doped systems. The perovskitelike structure ABO_3 of the manganites enables them to change their chemical composition within a wide range. Such chemical flexibility together with a strong coupling of the spin, charge, and orbital subsystems in the manganites lead to a very rich phase diagram involving various metallic, insulating, and magnetic phases.[1] It is well established that the ground state of the doped manganites is determined in many respects by an average cationic radius of the A site $\langle r_A \rangle$.[2] In the perovskite structure, the Mn ions occupy the B site being surrounded by oxygen octahedrons, while the rare-earth and alkaline-earth-metal elements occupy the A site between these octahedrons. The hybridization between Mn3de_g and O2p states form the electronically active band; this hybridization is strongly influenced by the internal pressure generated by A site substitution with ions of different radii. Thus the decrease of $\langle r_A \rangle$ leads to reduction of the hybridization between 3d and 2p states and, as a consequence, to reduction of the effective one-electron bandwidth W.[3] In such a case of narrow W, the kinetic energy of the itinerant e_g electrons is not large enough to enable charge delocalization, and the system can achieve a ferromagnetic (FM) or antiferromagnetic (AFM) insulating ground state. For example, the ground state of $Pr_{0.65}(Ca_xSr_{1-x})_{0.35}MnO_3$ and $La_{0.7-x}Nd_xPb_{0.3}MnO_3$ systems changes from the FM metallic state to the charge ordered AFM one with increasing of x.[4,5] The increase of $\langle r_A \rangle$ results in enhancement of the bandwidth W of the e_g electrons for Mn ions, which stabilizes the FM metallic state at low temperature due to the double exchange (DE) mechanism of the interaction between Mn^{3+} and Mn^{4+} ions.[6]

Another factor that is mainly responsible for features of the physical properties of the doped manganites is the disorder caused by the random chemical replacement of ions at the perovskite A sites (quenched disorder). The size difference between different ions located at the A sites induces local variations of the Mn-O-Mn bond angles and lengths. In particular, the latter leads to the random distribution of values and signs of the exchange coupling, since the bending of the Mn-O-Mn bonds modifies both FM DE and AFM superexchange coupling through Mn^{4+}-O-Mn^{3+} and Mn^{3+}-O-Mn^{3+} paths, respectively. The effect of random disorder under substitution is generally characterized by the parameter σ^2 defined as $\sigma^2=\langle r_A^2 \rangle - \langle r_A \rangle^2$.[7] The increase of σ^2 results in lowering of the Curie temperature T_C, deviation of the magnetic susceptibility from the Curie-Weiss behavior, and change of the colossal magnetoresistance (CMR) value. Moreover, the disorder of the size of the A site cations can induce the transition of the system from the FM metallic state to the spin-glass insulating one.[8]

It is obvious that the observed changes of the ground state in the manganites with doping arise from the competition of various interactions that have very similar energy scales in the system. At the same time, the energy balance can be so delicate that the system reveals instability towards phase

separation that can lead to a mixed-phase state with a complicated pattern that involves regions of two phases with different magnetic and electronic properties.[9] Often it is suggested that the phase separation phenomenon is induced by the introduction of the disorder in regions of parameters, where the competing electronic states are separated by the first-order transition[10,11] explaining the observed coexisting clusters of a micrometer size in some manganites. The coexisting clusters have equal charge densities, and their size is regulated by strength of the disorder. The outstanding peculiarity of the phase separation is that the state is very sensitive to external perturbations, such as magnetic and electric fields,[12] pressure,[13] x-ray,[14] and optical radiation.[15] As a result, manganites reveal various interesting phenomena, in particular, the existence of the inhomogeneous state and its easy reconstruction with modest magnetic field lead to CMR phenomena in the manganites.

Thus varying the type and ratio of the A cations in the perovskitelike manganites, it is possible to obtain compositions with the required magnetic and electrical properties. In this paper, we study the features of the magnetic and transport properties of the lanthanum manganite doped with Eu and Pb ions, $(La_{0.4}Eu_{0.6})_{0.7}Pb_{0.3}MnO_3$. The systematic study of the $(La_{1-y}Eu_y)_{0.7}Pb_{0.3}MnO_3$ series shows that the increase of y leads to lowering of the Curie temperature from $T_C = 350$ K for $y=0$ to $T_C=119$ K for $y=0.6$ (to be published elsewhere). In the composition interval $0 \leqslant y \leqslant 0.5$, the magnetic-phase transition is accompanied by the insulator-to-metal transition, and the CMR is observed near the transition. The $y=0.6$ crystal remains the insulating state down to the lowest temperatures, while the CMR effect is observed in a wide temperature range.

The choice of Pb ions was dictated by the peculiarity of the crystal-growth technique. Eu is of interest as an ion that reveals mixed valence Eu^{2+} and Eu^{3+} in oxides. Taking into consideration different electronic states and radii of these europium ions, one can expect that the charge transfer from Eu^{2+} or Mn^{3+} to Eu^{3+} results in the change of physical properties of the manganites. The charge transfer should be induced by the external perturbation, for example, by optical irradiation. Such a situation is realized in α-Fe_2O_3 crystals doped with europium ions.[16]

II. EXPERIMENTAL DETAILS

The single crystals of $(La_{0.4}Eu_{0.6})_{0.7}Pb_{0.3}MnO_3$ were grown by a method of spontaneous crystallization from solution in a melt. The mixture of PbO and PbF_2 was used as a solvent and at the same time it provided the Pb content in the crystals. The single crystals have a cubic shape of a typical dimension, $3\times3\times3$ mm^3. The crystals have black shiny surfaces and sharp edges. All measurements were carried out on well-polished platelike samples of a size of about $3\times3\times0.1$ mm^3.

The powder x-ray-diffraction patterns show that the crystal has a single phased perovskite-type structure without any impurity phase. All diffraction lines are assigned to the structure with a space group $P4/m$, the cell parameters are $a=b=3.8800(6)$ Å, $c=3.8705(4)$ Å, while the parent compound

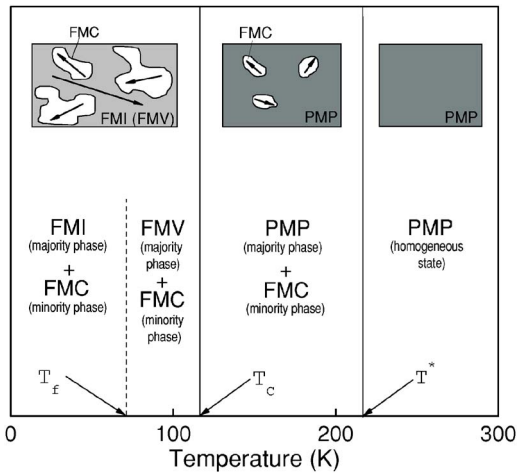

FIG. 1. Schematic temperature phase diagram of the $(La_{0.4}Eu_{0.6})_{0.7}Pb_{0.3}MnO_3$ system. PMP is the paramagnetic phase with the polaronic type of the conductivity; FMC, FMV, and FMI are ferromagnetic conducting, vibronic, and insulating phases, respectively. The upper panel represents simplified sketches of the proposed states in the crystal.

$La_{0.7}Pb_{0.3}MnO_3$ exhibits a rhombohedral structure with space group $R\bar{3}c$ and cell parameters $a=5.523\,70(1)$ Å and $c=13.402\,33(1)$ Å. The characterization by x-ray diffraction was also carried out versus temperature, from room temperature to 11 K. The measurements show that the symmetry remains unchanged in the whole temperature interval and no extra reflections have been detected.

The composition of the resulting crystals was confirmed by using x-ray fluorescence analysis. The identification of the phases and the determination of the lattice parameters were carried out using a powder x-ray diffractometer D8 ADVANCE (Brucker).

The transport and magnetic measurements were performed by means of a physical property measurement system (PPMS model 6000, Quantum Design) from 350 down to 2 K in magnetic fields up to 50 kOe. The magnetic-resonance measurements were performed with both a conventional cavity perturbation technique with microwave frequency $\nu=9$ GHz and with a spectrometer operating in the $\nu=24-80$-GHz frequency range with a pulsed external magnetic field of 0–80 kOe.

III. RESULTS AND DISCUSSION

The performed investigation clearly indicates that intrinsic magnetic inhomogeneities are present in the $(La_{0.4}Eu_{0.6})_{0.7}Pb_{0.3}MnO_3$ single crystal in a wide temperature range, although powder diffraction shows that the crystal appears to be single phase. The features in the behavior of the magnetic and transport properties are well described by assuming two different magnetic phases that differ in the electrical properties too. In order to facilitate the discussion of our results, we show in Fig. 1 a schematic phase diagram that displays the evolution of the inhomogeneous two-phase state with temperature. At high temperature, the material is in a

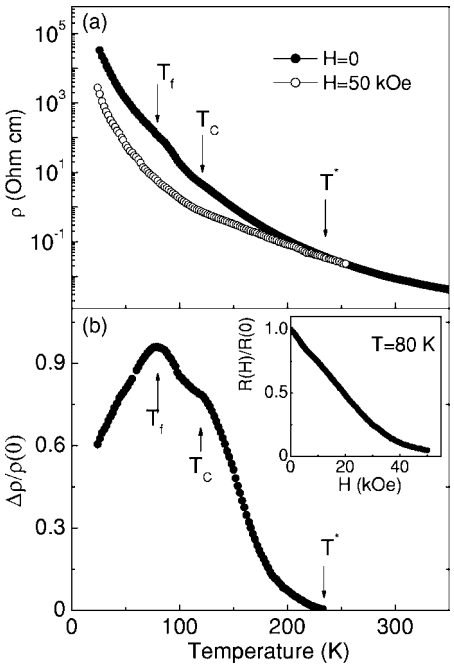

FIG. 2. (a) Temperature dependence of the resistivity ρ and (b) magnetoresistance $\Delta\rho/\rho(0)$ (b) for $(La_{0.4}Eu_{0.6})_{0.7}Pb_{0.3}MnO_3$. Inset: Magnetic-field dependence of the normalized resistivity $\rho(H)/\rho_0$ at $T=80$ K.

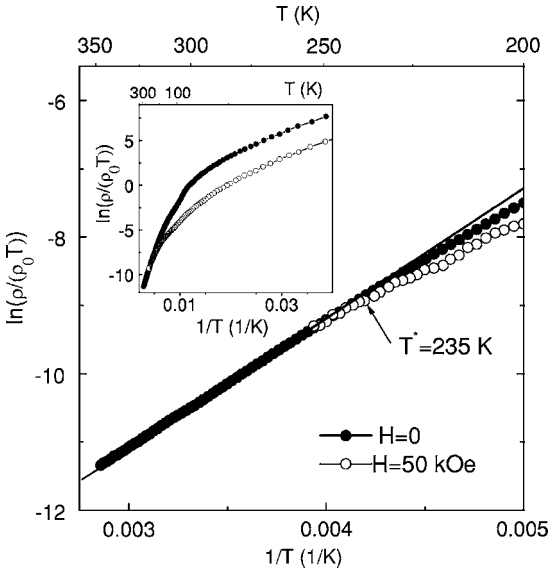

FIG. 3. Logarithm of ρ/T as a function of $1/T$ in magnetic fields $H=0$ and $H=50$ kOe. The solid line is a fit to a small polaron model, see text. The inset shows a complete view of the figure in the whole temperature range.

single paramagnetic phase exhibiting polaronic conductivity (PMP). With decreasing temperature a well conducting ferromagnetic minority phase (FMC) develops within the PMP matrix. Below the Curie temperature T_C, the PMP phase turns into a ferromagnetic vibronic majority phase (FMV). It transforms below T_f into an insulating ferromagnetic phase (FMI). This scenario will be derived in detail in the following sections based on the results of transport, magnetization, and magnetic-resonance measurements.

A. Transport properties

Figure 2(a) shows the temperature dependence of the resistivity ρ of the crystal in a field $H=50$ kOe and in zero field. The behavior of the magnetoresistance is displayed in Fig. 2(b). The sample does not reveal an insulator-to-metal transition, which is generally observed for doped manganites with the same hole concentration as for the crystal under investigation. At the same time the sample reveals the CMR effect at all temperatures below $T^*=235$ K. The CMR value $\Delta\rho/\rho(0)$ reaches a maximum value of 90% in a magnetic field of 50 kOe at $T_f\cong 80$ K. The inset in Fig. 2(a) shows that the CMR effect achieves almost saturation near 50 kOe.

Manganites are extremely complicated systems and it is typical for these materials that a variety of physical mechanisms control their behavior in different temperature ranges. The same picture is apparently realized for $(La_{0.4}Eu_{0.6})_{0.7}Pb_{0.3}MnO_3$. Over all, at high temperatures the temperature dependence of the resistivity follows reasonably well a model of small polaron hopping. This model predicts that $\rho=BT\exp(E_g/k_BT)$,[17] where B is a temperature independent coefficient, E_g is the activation energy, and k_B is the Boltzmann constant. The model is in good agreement with the data (Fig. 3). Note that the resistivity begins deviating from the small polaron type of behavior at the same temperature, where a noticeable CMR effect appears. This similarity indicates a common origin. It has been suggested[11] that the anomalous behavior found in the transport measurements at T^* are well above the magnetic ordering temperature is caused by the appearance of FMC clusters in a volume of the majority PMP phase. The FMC clusters of the minority phase have a higher conductivity than the PM matrix with polaronic type of conductivity. This assumption is supported by the following qualitative reasoning: The FM ordering in the mixed valence manganites arises due to the DE interaction, which results from the transfer of e_g electrons between the neighboring Mn^{3+} and Mn^{4+} ions through the Mn^{4+}-O-Mn^{3+}path. The value of the DE interaction is determined by the transfer integral of the e_g electrons hopping from Mn^{3+} to Mn^{4+} sites, which in turn is responsible for the electron motion. Thus there is a direct coupling between ferromagnetism and conductivity in the manganites. The A-site substitution with ions of different radii induces local distortions that are randomly distributed in the sample and lead to a great variation of the Mn-O-Mn bond angles and lengths. The distortions strongly modify the FM DE coupling through the Mn^{4+}-O-Mn^{3+} path, while the AFM superexchange interaction between neighboring Mn^{3+} ions through the Mn^{3+}-O-Mn^{3+} path is only marginally affected and therefore increases in importance. The crystal regions with the smaller bending of the Mn^{4+}-O-Mn^{3+} bonds have the stronger FM DE interaction resulting in the higher T_C and the higher electron mobility. The CMR phenomenon arises due to the growth of the FMC volume fraction in the external magnetic field. In the following sections the above assumptions will be confirmed by the data from the magnetization and magnetic-resonance measurements.

The next characteristic temperature, where anomalies of the transport and magnetotransport properties are observed is the Curie temperature (see Fig. 2 and inset of Fig. 3). The $\ln(\rho/T)$ curves in the inset of Fig. 3 reveal essential changes of the behavior in a temperature interval near T_C. This implies that arising of the FM ordering leads to a change of the electronic state in the system. Analysis of the $\ln(\rho/T)$ curves shows that another mechanism for conduction dominates in the sample below $T_f \cong 80$ K in comparison with the high-temperature region. At $T<T_f$ the experimental results are reasonably well fitted by Mott's variable-range hopping model. Within this model $\rho(T)=\rho_0 \exp[(T_0/T)^{1/4}]$,[18] where ρ_0 is a pre-exponential factor and T_0 is related to the density of states at the Fermi level. Such behavior of the resistivity is typical for disorder and a topologically inhomogeneous medium.

The features in the behavior of ρ and $\Delta\rho/\rho(0)$ that are observed for $T_f<T<T_C$ are consistent with those in the literature.[19] It has been suggested[20] that on cooling sample through T_C, the transition from the PMP state to the FMI state passes through an intermediate more conductive FMV state. By analogy, we identify the interval $T_f<T<T_C$ with a region where the FMV state appears in the majority phase of the crystal. As a rule, this state is realized for manganites in a compositional interval between an AFM insulating state and a FM metallic state. It is clear that the composition of the $(La_{0.4}Eu_{0.6})_{0.7}Pb_{0.3}MnO_3$ crystal being under investigation satisfies this condition. Indeed we observe the transition in the FM metallic state for the samples $(La_{1-y}Eu_y)_{0.7}Pb_{0.3}MnO_3$ with $y=0-0.4$. For the $y=0.5$ sample, after the insulator-to-metal transition there is an upturn in its resistivity towards lower temperature indicating insulating behavior. At $y=0.6$, only a slight change in the insulator type of conductivity takes place right below T_C. Thus the Eu substitution for La ions in $La_{0.7}Pb_{0.3}MnO_3$ leads to the suppression of the FM state. Moreover, the system being initially in a metallic state tends to an insulating ground state at low temperature.

One more indication for an inhomogeneous sample is its nonlinear transport properties. Indeed, it has been widely shown that nonlinear conduction in the various mixed-valent manganites is caused by the transformation of the multiphase state under current perturbation.[12,21] The nonlinear behavior of current-voltage (*I-V*) characteristics (Fig. 4) for our sample is observed in the whole temperature range, where the CMR effect occurs. However, the most significant nonlinear conduction occurs in the sample at temperatures near T_f. Figure 4 shows the *I-V* characteristics in a magnetic field at $T=80$ K. The application of it strongly modifies the *I-V* characteristics restoring its linear behavior above 30 kOe. Therefore the changes are not only related to the increasing of the conductivity with increasing magnetic field, but also the character of the nonlinearity is modified. We will return to the discussion of this question later.

B. Magnetization measurements

Because the charge transport in the manganites is intimately linked with their magnetic state, we have investigated the magnetic properties of the material. We have carried out magnetization measurements on our sample both below and above T_C in various magnetic fields. Figure 5 shows the temperature dependence of the inverse susceptibility χ^{-1}. It follows a Curie-Weiss law at high temperature; however, there is a change in the low-temperature behavior, when χ^{-1} lies substantially above the Curie-Weiss limit as T_C is approached from high temperature. Such behavior strongly suggests effects of spin clustering when local ferromagnetic regions exist above T_C.[22] This conclusion is consistent with our assumption made in the previous section: the peculiarities of transport and magnetotransport properties below T^* are related to the appearance of well conducting FM clusters. One should notice, that the deviation of χ^{-1} from the Curie-Weiss law starts at the same temperature, where the CMR effect becomes clearly visible.

The inhomogeneous state of the sample below T_C is confirmed by the measurements of the magnetization M. The low-field magnetization was measured by warming up in low field after cooling down from room temperature (i) first without a magnetic field [zero-field cooled (ZFC)] and (ii) sub-

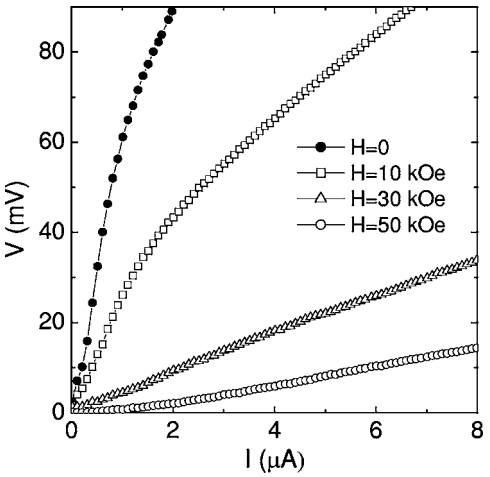

FIG. 4. Current-voltage (*I-V*) characteristics measured in different magnetic fields at 80 K.

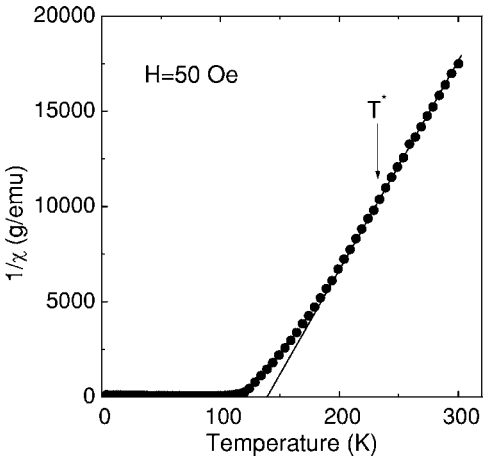

FIG. 5. Inverse magnetic susceptibility χ^{-1} vs temperature at $H=50$ Oe.

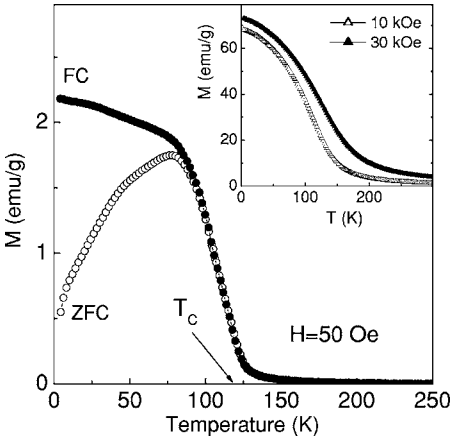

FIG. 6. FC and ZFC dc magnetization measured as a function of temperature at $H=50$ Oe. Inset: Temperature dependence of M in applied fields of 10 and 30 kOe.

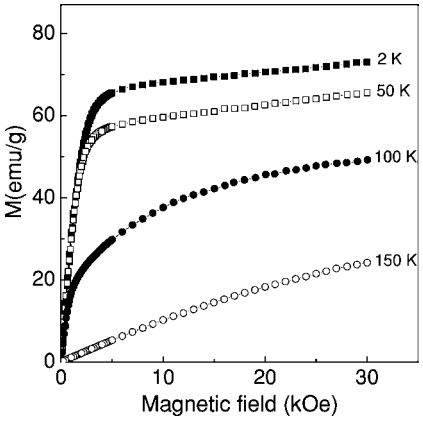

FIG. 7. Magnetic-field dependence of the magnetization at various temperatures $2<T<150$ K.

sequently in an applied field [field cooled (FC)] of 50 Oe (Fig. 6). As shown, the difference between the FC and ZFC magnetization increases with decreasing temperature. Moreover, the ZFC curve shows a peak, and below the peak M significantly decreases with decreasing temperature. A λ-shape trace, the presence of a maximum at the temperature T_f, and a thermomagnetic irreversibility below T_f are the characteristic features of the ZFC magnetization of a magnetically inhomogeneity system with a spin-glass-like nature.[23] In our case, the sample is not actually in the canonical spin-glass state, however, the observed behavior can arise from ferromagnetic clusters, whose moments are gradually blocked with decreasing temperature below T_f. For example, such a behavior may be observed if there exist two phases in the form of FM and AFM clusters in the sample. The spin-glass-like behavior of the magnetization is possible when FM regions of a minority phase are embedded in a FM background of the majority phase, and these different FM phases are coupled at a phase boundary by exchange interactions that differ in sign and value from the intraphase interactions. We have many reasons to believe that such a state is realized in the manganites with A-site cationic disorder, favoring strong competition between the FM and AFM interactions in the system.[10,24]

The inset of Fig. 6 shows the temperature dependence of M at larger magnetic fields $H=10$ kOe and $H=30$ kOe. The curves have forms that are typical of ferromagnets. The behavior of M versus magnetic field is also typical for a sample with FM ordering, Fig. 7. However, we can see that the sample does not reach saturation even at T as low as to $T=2$ K. The value of the saturation moment obtained from the extrapolation of the magnetization curve to $T=0$ K at $H=30$ kOe amounts to $\sigma_{\text{exp}}=3.5\mu_B$ per formula unit. This value is smaller than the nominal ferromagnetic saturation moment $\sigma_S=3.7\mu_B$ at $T=0$ K and $H=\infty$ that is expected for $x=0.3$ in $(La_{1-y}Eu_y)_{1-x}Pb_xMnO_3$. At the same time, for $(La_{1-y}Eu_y)_{0.7}Pb_{0.3}MnO_3$ crystals with smaller Eu doping ($y=0,0.2,0.4$), values of the magnetic moments at $T=2$ K and $H=30$ kOe are essentially identical to the nominal ferromagnetic saturation moment. Therefore in our case ($y=0.6$) the necessary field to obtain saturation is much stronger than the applied field $H=30$ kOe. Hence the data are consistent with the assumption of an inhomogeneous sample. Indeed, the spin state with competing FM and AFM exchange coupling in the volume of the sample is harder to be magnetized than a homogeneous state with FM long-range spin order. It is possible that a small fraction of AFM phase is contained in the sample volume.

C. Magnetic-resonance measurements

The method of electron magnetic resonance is an effective tool for probing inhomogeneities in magnetic materials, allowing the determination of the magnetic states of the coexisting phases and their behavior for various temperatures and magnetic fields.

For the analysis of the experimental spectra recorded at microwave frequencies 9, 26, and 54 GHz we applied a fitting procedure based on Lorentzian lines. It became clear that the observed spectra could be fitted satisfactorily, if we assumed the presence of two absorption lines. Figure 8 shows the typical magnetic-resonance spectrum recorded at the microwave frequency $\nu=26$ GHz and the temperature 80 K and the best result of the two-Lorentzian lines analysis for this spectrum. With decreasing temperature, two peaks are confidently detected in the spectra near 220 K. This temperature is close to the temperatures where anomalies in χ^{-1} and the transport properties appear in the system. Figure 9 shows the temperature dependence of the resonance fields H_r^1, H_r^2 (a) and linewidths $\Delta H^1, \Delta H^2$ (b) for both absorption lines in the magnetic-resonance spectra. The measurements were performed at a microwave frequency $\nu=26$ GHz. The ratio of the integrated intensities (A_2/A_1) of the resonance lines versus temperature is presented in Fig. 9(c). We suppose that the observed lines are related to the magnetic-resonance absorptions in the two different phases coexisting in the sample volume. The A_2/A_1 value reflects reasonably well the evolution of the mixed two-phase state (changes of the volume fractions and magnetization values of the phases) in the sample, although we have to keep in mind that various mechanisms make contributions to the intensity of the absorption lines.[25] Analyzing the behavior of the resonance

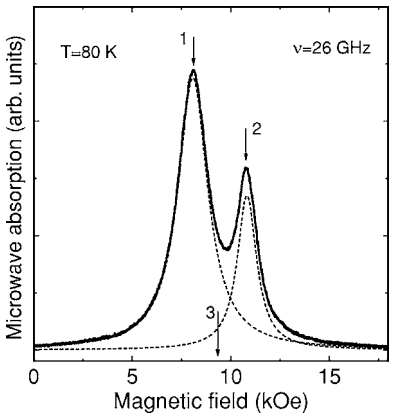

FIG. 8. Magnetic-resonance spectrum recorded at microwave frequency $\nu=26$ GHz and $T=80$ K. The solid line is the experimental absorption line, dashed lines are the best fitting by two Lorentzian absorption lines. The arrows indicate the position of the two observed absorption lines (1 and 2) and the position that is determined by the expression $H_r=\nu/\gamma$ related to a spherical, isotropic, and homogeneous ferromagnet (3).

lines versus temperature and frequency, Figs. 9 and 10, we can obtain information on the magnetic state of the coexisting phases and the magnetic interactions between regions of the different phases. We find that the resonance data are consistent with the transport and magnetization measurements thus justifying the proposed scenario in the phase diagram of Fig. 1.

When $T>T^*$, the sample is in the homogeneous PMP state. Therefore only a single absorption line is observed in the spectrum. Below T^*, FMC clusters of the minority phase appear in the volume of the majority PMP phase and an additional line corresponding to the FM resonance absorption arises in the spectrum at a higher magnetic field than the PM line. As the temperature is lowered further, the intensity of this line, A_2, increases due to the increasing volume fraction of the FMC phase and its increasing magnetization. However, the minority FMC phase does not percolate. On cooling through T_C, the sample undergoes a transition from the PMP to the FM state. This transition occurs in the volume of the majority phase. The difference between the FMV and FMI state, which is revealed in the transport measurements, is not observed in the magnetic-resonance spectra. Below T_C two FM phases, FMC and FMI (or FMV), coexist in the sample. The FM regions of the different phases have different directions of the magnetic moments, which are frozen due to the difference of the magnetic interactions at the boundary of the phases from the intraphase interactions. The latter give rise to the spin-glass-like behavior of the system.

It is necessary to pay attention to the following features in behavior of the magnetic resonance spectra: First, as the temperature decreases from T_C, the resonance field of the absorption line from the minority phase, H_r^2, shifts to a higher magnetic field, while H_r^1, which corresponds to the absorption line from the majority phase, decreases. The line "splitting" increases with the increasing microwave frequency (see Fig. 10). Second, the ratio of the absorption line intensities (A_2/A_1) is frequency dependent. Figure 11 shows that A_2/A_1

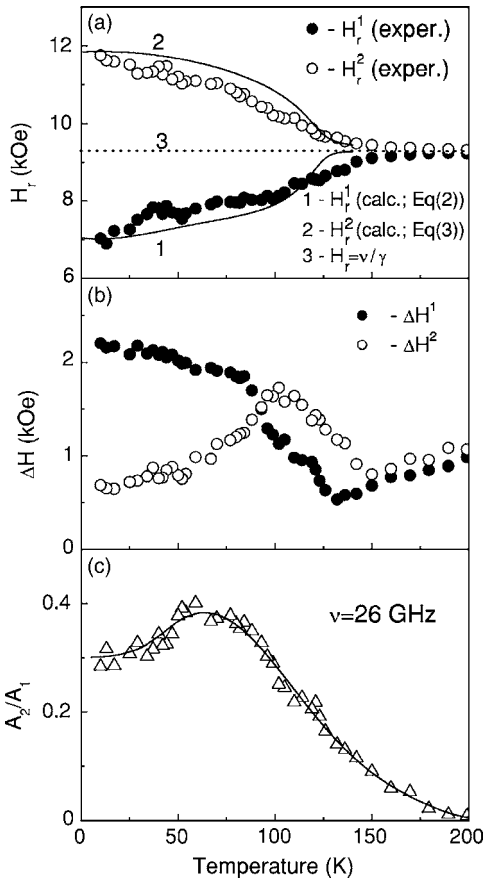

FIG. 9. Temperature dependence of the resonance parameters of two absorption lines in the magnetic resonance spectra ($\nu=26$ GHz). (a) Symbols denote the experimental data for resonance fields H_r^1 (majority phase) and H_r^2 (minority phase), solid lines 1 and 2 represent the model calculation given by Eqs. (2) and (3), respectively. The dotted line 3 indicates the $H_r=\nu/\gamma$ dependence related to a spherical, isotropic, and homogeneous ferromagnet. (b) Dependence of the linewidths ΔH^1, ΔH^2 on temperature. (c) Ratio of the integrated intensities A_2/A_1 of the two resonance lines vs temperature.

increases with the increasing microwave frequency. The behavior of the resonance field H_r^1 and other resonance parameters below T_C are typical for those manganite compounds investigated earlier that undergo a FM transition.[25] H_r^1 depends mainly on the magnetization of the majority phase M_1 that changes with temperature and external magnetic field. The behavior of H_r^2 can be explained in the framework of the above assumption as follows: The minority phase in the sample is composed of disconnected FM regions, coupled with the FM background at the interfaces separating the two phases. They are mostly coupled by antiferromagnetic exchange interactions. The dependence of A_2/A_1 on the microwave frequency ν is interpreted as a change of the volume fractions of the coexisting phases with the magnetic field (the increasing of ν results in the increasing of the magnetic field where the resonance absorption lines are observed). To demonstrate the validity of the conclusions given above, we derive below a simple model reproducing all qualitative features of the experimental spectra for the studied two-phase system.

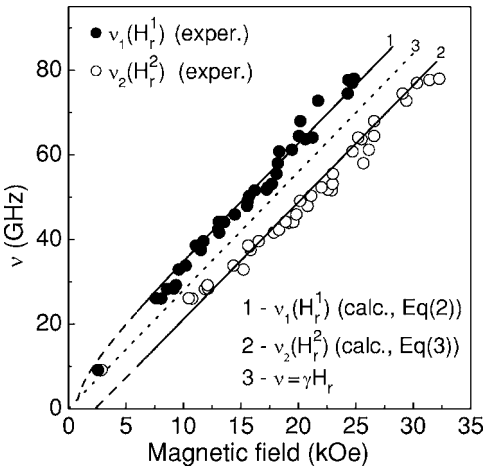

FIG. 10. Frequency-field dependencies for the two absorption lines in the magnetic resonance spectra at $T=80$ K. Symbols are experimental points $\nu_1(H_r^1)$ and $\nu_2(H_r^2)$, solid lines 1 and 2 represent dependencies given by Eqs. (2) and (3), respectively. Dashed lines correspond to conditions, where the magnetic field $H<H_{sat}$ and Eqs. (2) and (3) are not valid. The dotted line 3 is the dependence for the spherical isotropic homogeneous ferromagnet, $\nu=\gamma H_r$.

D. Magnetic-resonance spectra of the two-phase system: A simple model

According to the experiment, the sample has the shape of a thin plate and the field is applied with the plane of the plate. The disconnected regions of the minority FM phase with the volume V_2 are embedded in the volume V_1 of the majority FM phase. The majority and minority phases with the magnetizations M_1 and M_2, respectively, are coupled to each other at the interface. The total free energy per unit volume of the system can be written as

$$E=\frac{1}{1+x}\{-\bar{M}_1\bar{H}+K_{A1}+K_{S1}\}+\frac{x}{1+x}\{-\bar{M}_2\bar{H}+K_{A2}+K_{S2}\}$$
$$-J_{eff}\bar{M}_1\bar{M}_2, \quad (1)$$

where $x=V_2/V_1$, K_{A1} and K_{A2} are the energy of the magnetocrystalline anisotropies, K_{S1} and K_{S2} are the demagnetization energies originating from the shape of the sample and the topology of the inhomogeneity. Here, indexes 1 and 2 denote the majority and minority phases, respectively. The sign and the value of the coupling parameter J_{eff} describe the character (FM or AFM) and strength of the coupling between the phases. If J_{eff} is negative, the energy is minimal for AFM coupling. It is obvious that J_{eff} is a function of the area of the boundary separating the different phases. This area depends on the shape of the minority phase but not so much on V_2. It is well established that the state with magnetic-phase separation in the manganites can reveal a very intricate physical geometry that depends strongly on temperature and magnetic field,[26,27] which too complicate the functional relationship between J_{eff} and x. Moreover, the complex topology of the magnetically inhomogeneous state makes it difficult to calculate the energy of the demagnetizing fields.

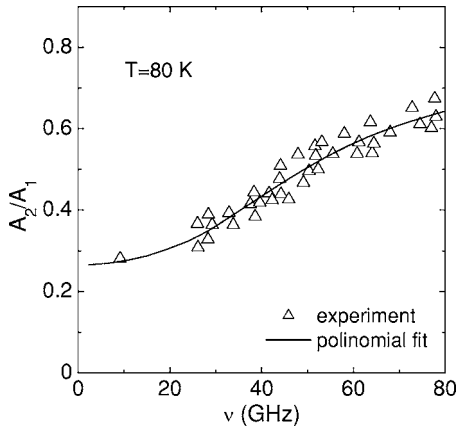

FIG. 11. Ratio of the integrated intensities A_2/A_1 of two resonance lines vs microwave frequency. Symbols are the experimental points, the solid line is a polynomial fit.

To simplify our model we have considered only a strong demagnetizing field for the majority phase, originating from the platelike shape of the sample. We have neglected the demagnetizing effects related to the topology of the magnetic inhomogeneity. Moreover, we have not considered the energies of the magnetic crystallographic anisotropy K_{A1} and K_{A2}. Indeed, it is well known that the magnetic anisotropy of the three-dimensional (3D) perovskitelike manganites is generally small. For our sample, a change of the magnetic-field direction relative to the crystallographic axes of the sample shifts both absorption lines less than 100 Oe at $T=80$ K, implying that the magnetocrystalline anisotropy does not influence the behavior of the magnetic-resonance spectra significantly.

With all these considerations, finding the equilibrium conditions for $\bar{M}_1$ and $\bar{M}_2$ and solving the linearized equations of motion one can obtain the dispersion relation for the two absorption peaks observed in the magnetic-resonance spectrum of the assumed two-phase system. The resonance conditions for the majority and minority phase will be approximately given by the following equations:

$$\left(\frac{\nu_1}{\gamma}\right)^2\approx[H_r^1+(1+x)J_{eff}M_2][H_r^1+(1+x)J_{eff}M_2+4\pi M_1], \quad (2)$$

and

$$\frac{\nu_2}{\gamma}\approx H_r^2+\left(\frac{1+x}{x}\right)J_{eff}M_1, \quad (3)$$

where γ is the gyromagnetic ratio, and H_r^1 and H_r^2 are the resonance fields of the absorption lines from the majority and minority phases, respectively. Equations (2) and (3) were derived under the assumption that $\bar{M}_1$ and $\bar{M}_2$ are parallel, i.e., at $H>H_{sat}$, where H_{sat} is the saturation field. Solving these equations we obtained the corresponding dependencies of H_r^1 and H_r^2 on temperature and microwave frequency, as shown by the solid lines in Figs. 9 and 10. The parameters used in the computation were selected close to the experiment conditions. Since $\bar{M}_1$ and $\bar{M}_2$ are a function of temperature and magnetic field, we approximated their dependence by Bril-

louin functions with Curie temperatures 119 and 200 K, respectively. The principal fitting parameter of the model is J_{eff}. Since our experimental methods do not allow any conclusion about the geometry of the two-phase state, we used the simple condition $J_{eff}=C\cdot x^{2/3}$ that is valid for a spherical shape of the clusters of the minority phase. To obtain the dependencies that reproduce the features in the behavior of H_r^1 and H_r^2 (see Figs. 9 and 10), we have to assign negative values to C corresponding to AFM exchange coupling between the coexisting phases. Moreover, we assume that x changes with temperature and magnetic field. In the simulation, we replaced the parameter x by the experimentally determined ratio A_2/A_1, because it is reasonable to assume that the change of the intensities of the lines occurs mainly due to the change of the phase volumes with T and ν. The model calculations are shown in Figs. 9 and 10 for $C=-2.1$. The dashed lines in Fig. 10 correspond to the interval of the magnetic field, where $H<H_{sat}$, where Eqs. (2) and (3) are not valid.

The comparison of the experimental data and the calculated curves demonstrates that the proposed simple model confirms qualitatively our assumptions based on the transport, magnetization and magnetic-resonance measurements, although the real picture is evidently more complicated. Indeed, there are distributions in the dimension and shape of the regions of the minority phase that result in a distribution of the J_{eff} value. In particular, it can lead to an additional growth of the linewidths of the resonance absorptions peaks in the experiment. Also it can explain the pronounced deviation of the experimental and calculated dependencies at low magnetic fields (Fig. 10). Actually, H_{sat} differs for different regions of the minority phase, and it is necessary to examine the state, when $\bar{M}_1$ and $\bar{M}_2$ are not parallel. In this case, Eqs. (2) and (3) are inapplicable. It is probable that some of the features in the experimental results, for example a strong spread of the experimental points are related to magnetic relaxation processes, i.e., to dynamic properties of the phase-separated state.[24]

E. Magnetic-field-driven electrical transport

Finally, we would like to discuss the electrical transport properties in the studied manganite. The two-phase model discussed above does not allow a direct calculation of the resistivity. However, it is clear that the observed transport and magnetotransport phenomena are related to the sensitivity of the inhomogeneous state on changes of temperature and magnetic field. The CMR effect originates from the growing of the volume fraction of the more conducting minority phase with increasing magnetic field. Although, in general one should also consider the possibility that the conductivity of the two-phase system is sensitive to changes of the geometry of the two-phase state.[28]

Based on the assumptions concerning the structure of the magnetic inhomogeneities in the sample one may assume that the magnetoresistance may be influenced by spin-polarized tunneling.[29] Then the conductivity of the FM regions that are separated by tunnel barriers (AFM, insulating in our case) depends on the relative direction of the magnetization in these regions. Therefore the tunneling magnetoresistance should be observed in low magnetic fields $H<H_{sat}$. However, we did not experimentally detect any pronounced features that can be attributed to spin-dependent tunneling [see the inset in Fig. 2(b)].

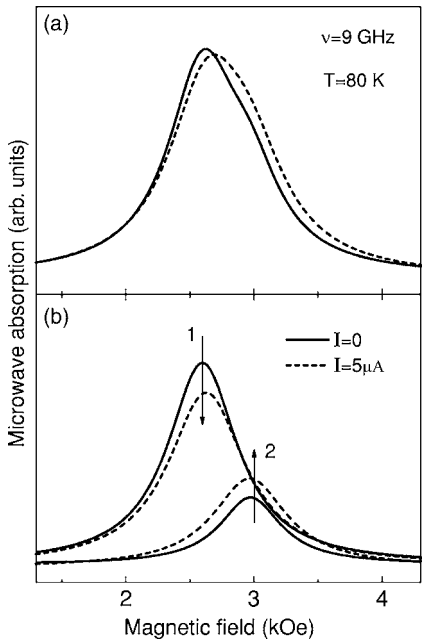

FIG. 12. (a) Magnetic-resonance spectra recorded without (solid line) and with dc current perturbation (dashed line); $\nu=9$ GHz and $T=80$ K. (b) The corresponding change of the two absorption lines 1 and 2 observed in the spectrum as a result of the current influence. The arrows indicate the decreasing and increasing of the intensity of the magnetic-resonance absorption from the majority (1) and minority (2) phases, respectively.

A simple scenario that allows explaining the nonlinear conduction implies the sensitivity of the intrinsic inhomogeneity on electric currents. The applied current may influence the relative volumes of the coexisting phases and/or their geometry. Both variants result in a nonlinear *I-V* characteristic. We have carried out experiments to determine which mechanism is more probable. The magnetic-resonance spectra have been investigated under passing of dc current through the sample. We have used the microwave irradiation with the frequency of 9 GHz, because in this case the absorption spectra are observed in low magnetic field ($H_r^1, H_r^2 < 3$ kOe), when the pronounced nonlinear electrical transport occurs in the sample. Figure 12 shows the dc current effect on the magnetic-resonance spectrum. Increasing I, we find that the intensity of the line of the minority phase, A_2, increases, while that of A_1 decreases. Such a behavior suggests that the current induces the growth of the volume fraction of the more conductive minority phase. Decreasing the voltage across the sample results in a nonlinear regime of the conductivity (see Fig. 4).

We are not going to discuss the possible mechanisms on how the current influences the phase separation here. In low magnetic fields, an increase in I results in a decrease of dV/dI indicating the growth of the volume fraction of the more conductive phase with I and H. Therefore the effects of

current and magnetic field have the same sign. In contrast, in high magnetic fields, dV/dI increases (see Fig. 4) suggesting that the increase in I results in a decrease of the more conductive phase, i.e., the effects of current and field are opposite to each other. Thus in spite of the fact that these effects must be fundamentally different in nature (the magnetic field affects the spin subsystem, while the electric field interacts with the induced polarization) they are intimately connected with each other. From a practical point of view, the crystal $(La_{0.4}Eu_{0.6})_{0.7}Pb_{0.3}MnO_3$ represents a system, where the current-voltage characteristics are controlled by a magnetic field.

IV. CONCLUSION

In this work we have investigated the physical properties of a single crystal of $(La_{0.4}Eu_{0.6})_{0.7}Pb_{0.3}MnO_3$. The measurements of the transport properties together with magnetization and magnetic-resonance measurements confirm the coexistence of two magnetic phases in the crystal.

The data support the following scenario for the evolution of the inhomogeneous state and the behavior of the physical properties related to the phase separation. From high temperature down to $T^* \cong 235$ K the sample is in a homogeneous PMP state with a polaron type conductivity. At T^*, FMC clusters having higher conductivity than the PMP matrix appear in the sample volume. The appearance of the FMC regions is correlated with the appearance of a FM absorption line in the magnetic-resonance spectra and with the anomalous behavior found in the transport and magnetotransport measurements. As temperature decreases further, the size and/or number of the FM regions increases, but the minority phase does not percolate. At $T_C = 119$ K, FM ordering appears in the majority phase and below T_C the coexistence of two different FM phases takes place in the sample. With respect to the magnetic properties, these FM phases are observed to be spatially separated due to the fact that the couplings at the phase boundaries have mostly AFM character, although the value of these couplings can strongly fluctuate. Therefore at lower temperature the regions of the FMC minority phase are blocked with random magnetization directions in the volume of the FM background of the majority phase, that, in its in turn, is responsible for the observed magnetic glassylike behavior. It should be stressed that in our case the coexistence of the different FM phases occurs, as opposite to the standard phase separation picture, when the FM metallic and AFM charge ordered insulating phases coexist in the sample.[30]

The phase-separation state observed in $(La_{0.4}Eu_{0.6})_{0.7}Pb_{0.3}MnO_3$ manganite can arise from the quenched disorder resulting from complex substitution of A site cations in the perovskite structure of the manganite. This disorder, in turn, induces local variations of the Mn-O-Mn bond angles and lengths and favors a random distribution of competing FM and AFM exchange interactions in the crystal volume.

Within the two-phase model, the CMR and the magnetic-field-driven nonlinear transport can be explained under the assumption that the inhomogeneous state is sensitive to the external magnetic field and current. The application of magnetic field or current leads to a change of the volume fraction of more conducting minority FM phase, resulting in change of the whole sample conductivity. As a result CMR and nonlinear transport occur in the system.

ACKNOWLEDGMENTS

This work was supported by the KRSF-RFBR "Enisey2005" Grant No. 05-02-97708-a. N.V. thanks the DAAD Foundation for financial support (Grant No. A/03/06137) during his work at the Physics Department E21 at the Technical University of Munich.

[1] A. Moreo, S. Yunoki, and E. Dagotto, Science **283**, 2034 (1999).
[2] H. Y. Hwang, S.-W. Cheong, P. G. Radaelli, M. Marezio, and B. Batlogg, Phys. Rev. Lett. **75**, 914 (1995).
[3] J. B. Torrance, P. Lacorre, A. I. Nazzal, E. J. Ansaldo, and Ch. Niedermayer, Phys. Rev. B **45**, R8209 (1992).
[4] H. Yoshizawa, R. Kajimoto, H. Kawano, Y. Tomioka, and Y. Tokura, Phys. Rev. B **55**, 2729 (1997).
[5] N. Ghosh, S. Elizabeth, H. L. Bhat, U. K. Rossler, K. Nenkov, S. Rossler, K. Dörr, and K. H. Müller, Phys. Rev. B **70**, 184436 (2004).
[6] P.-G. de Gennes, Phys. Rev. **118**, 141 (1960).
[7] L. M. Rodriguez-Martinez and J. P. Attfield, Phys. Rev. B **54**, R15622 (1996).
[8] A. Maignan, C. Martin, G. Van Tendeloo, M. Hervieu, and B. Raveau, Phys. Rev. B **60**, 15214 (1999).
[9] D. Dagotto, T. Hotta, and A. Moreo, Phys. Rep. **344**, 1 (2001).
[10] A. Moreo and E. Dagotto, J. Magn. Magn. Mater. **226-230**, 763 (2001).
[11] E. Dagotto, J. Burgy, and A. Moreo, Solid State Commun. **126**, 9 (2003).
[12] R. C. Budhani, N. K. Pandey, P. Padhan, S. Srivastava, and R. P. S. M. Lobo, Phys. Rev. B **65**, 014429 (2002).
[13] V. Markovich, I. Fita, R. Puzniak, M. I. Tsindlekht, A. Wisniewski, and G. Gorodetsky, Phys. Rev. B **66**, 094409 (2002).
[14] V. Kiryukhin, D. Casa, J. P. Hill, B. Keimer, V. Vigliante, Y. Tomioka, and Y. Tokura, Nature (London) **386**, 813 (1997).
[15] K. Ogawa, W. Wei, K. Miyano, Y. Tomioka, and Y. Tokura, Phys. Rev. B **57**, R15033 (1998).
[16] G. S. Patrin, N. V. Volkov, and G. A. Petrakovskii, Sov. Phys. JETP **74**, 337 (1992).
[17] T. Holstein, Ann. Phys. (N.Y.) **8**, 325 (1959).
[18] J. M. D. Coey, M. Viret, and S. von Molnar, Adv. Phys. **48**, 167 (1999).
[19] G.-L. Liu, J.-S. Zhou, and J. B. Goodenough, Phys. Rev. B **70**, 224421 (2004).
[20] J.-S. Zhou and J. B. Goodenough, Phys. Rev. B **68**, 054403 (2003).
[21] A. Guha, A. K. Raychaudhuri, A. R. Raju, and C. N. R. Rao,

Phys. Rev. B **62**, 5320 (2000).
[22] L. M. Rodriguez-Martinez and J. P. Attfield, Phys. Rev. B **54**, R15622 (1996).
[23] C. Y. Huang, J. Magn. Magn. Mater. **51**, 1 (1985).
[24] R. S. Freitas, L. Ghivelder, F. Damay, F. Dias, and L. F. Cohen, Phys. Rev. B **64**, 144404 (2001).
[25] N. V. Volkov, G. A. Petrakovskii, V. N. Vasiliev, D. A. Velikanov, K. A. Sablina, and K. G. Patrin, Physica B **324**, 254 (2002).
[26] Ch. Simon, S. Mercone, N. Guiblin, C. Martin, A. Brûlet, and G. Andre, Phys. Rev. Lett. **89**, 207202 (2002).
[27] M. Viret, F. Ott, J. P. Renard, H. Glättli, L. Pinsard-Gaudart, and A. Revcolevschi, Phys. Rev. Lett. **93**, 217402 (2004).
[28] A. N. Lagarkov and A. K. Sarychev, Phys. Rev. B **53**, 6318 (1996).
[29] Y. Yuzhelevski, V. Markovich, V. Dikovsky, E. Rozenberg, G. Gorodetsky, G. Jung, D. A. Shulyatev, and Y. M. Mukovskii, Phys. Rev. B **64**, 224428 (2001).
[30] P. G. Radaelli, R. M. Ibberson, D. N. Argyriou, H. Casalta, K. H. Andersen, S.-W. Cheong, and J. F. Mitchell, Phys. Rev. B **63**, 172419 (2001).